

# Evolutionarily optimized ultrahigh-Q photonic crystal nanocavity

Ulagalandha Perumal Dharanipathy<sup>1</sup>, Momchil Minkov<sup>2</sup>, Mario Tonin<sup>1</sup>,

Vincenzo Savona<sup>2</sup> and Romuald Houdré<sup>1</sup>

<sup>1</sup>*Institut de Physique de la Matière Condensée, Ecole Polytechnique Fédérale de Lausanne (EPFL), Station 3, CH-1015 Lausanne, Switzerland*

<sup>2</sup>*Institut de Théorie des Phénomènes Physiques, Ecole Polytechnique Fédérale de Lausanne (EPFL), Station 3, CH-1015 Lausanne, Switzerland*

Photonic crystal (PhC) nanocavities are promising building blocks of future integrated photonic circuits<sup>1-4</sup>. Owing to the high ratio between quality factor ( $Q$ ) and modal volume ( $V$ ), they can greatly enhance optical nonlinearities and radiation-matter interaction, establishing a new paradigm in cavity quantum electrodynamics<sup>5-7</sup>. However, only few specific designs have reached measured  $Q$ -factors exceeding one million<sup>8-10</sup>, mostly as a result of a heuristic optimization. Here, we develop a global optimization procedure based on an evolutionary algorithm that, if applied to simple moderate- $Q$  nanocavities<sup>11-15</sup>, can enhance their measured quality factor by over one decade, approaching the one-million range. In particular, we optimize and experimentally characterize a  $H0$  PhC nanocavity<sup>1,13,15,16</sup>, demonstrating a measured  $Q$ -factor reaching 418,000 combined with a modal volume  $V = 0.35 \left(\frac{\lambda}{n}\right)^3$ . This cavity ranks among those with the highest  $\frac{Q}{V}$  ratios ever demonstrated, while being spatially much more compact than ultrahigh- $Q$  designs and thus optimal for integration in photonic circuits<sup>8-10</sup>. It displays nonlinear effects in the  $\mu\text{W}$  power range,

**including high-contrast optical bistability at record-low threshold power in silicon. We highlight the versatility of the optimization procedure by further devising an alternate  $H0$  design with a smaller modal volume of  $V = 0.26\left(\frac{\lambda}{n}\right)^3$  and a measured Q-factor of 260,000.**

The optimization of the quality factor has been a primary objective of PhC cavity design until recently. In particular, the early pioneering investigations showed that, by appropriately shifting the positions and radii of holes adjacent to the cavity, the Q-factor could increase by orders of magnitude<sup>11,12</sup> while leaving the modal volume almost unchanged. Subsequent work<sup>17-19</sup> produced few ultrahigh-Q designs, however at the cost of increasingly complex and spatially extended cavity patterns. At the same time, it became clear that the quality factor in high-Q cavities is limited by extrinsic losses due to fabrication disorder<sup>10,20,21</sup> along with residual material losses<sup>22</sup>. A more beneficial strategy thus consists in optimizing the Q-factor together with other important features, such as small modal volume<sup>13-15</sup> – in order to enhance optical nonlinearities and light-matter interaction<sup>5-7,23</sup> – and spatial compactness, implying an increased ease of integration in photonic circuits. Within this perspective, the huge parameter space characterizing typical cavity designs remains largely unexplored, mostly due to the high computational cost of typical simulation tools, effectively limiting the optimization procedure to a necessarily incomplete heuristic search. Here, we overcome this difficulty by adopting a computationally fast simulation method – specifically, the Guided Mode Expansion (GME)<sup>24</sup>. GME reliably predicts mode frequencies and Q-factors within minutes of computational time on a PC, by compromising only slightly on accuracy if compared to the much slower first principle simulation tools. The simulation can then be associated to a global

optimization procedure to be used for the exploration of the entire parameter space. The procedure chosen here is a genetic optimization algorithm (see supplementary information), which relies on a wide array of evolution-inspired techniques to determine an absolute extremum of the chosen objective function.

Our objective is to start from a simple and spatially compact PhC nanocavity chosen among those that are commonly considered as low- to moderate- $Q^{11-15}$  and, by optimizing a small number of parameters, show that it can reach measured  $\frac{Q}{V}$  values close to the record-high ones characterizing typical ultrahigh- $Q$  designs<sup>8-10</sup>. To this purpose, we select the  $H0$  cavity design<sup>13,15</sup>, which has the smallest known modal volume among 2D PhC structures. The optimized design of our cavity is illustrated in Fig. 1a. The thickness of the PhC slab is  $0.5a$  while the radius of each hole is  $0.25a$  ( $a$  is the lattice constant) and the refractive index is  $n = 3.46$ . The basic  $H0$  design consists of two holes shifted away from their original positions by an amount  $S_{1x}$  (see Fig. 1a). The optimization is carried out by allowing for four more shifts of neighbouring holes along the x-axis and two shifts along the y-axis, as shown in Fig. 1a. The objective function of the evolutionary optimization was the cavity quality factor, while reasonable restrictions were imposed on the magnitudes of the shifts in order to limit the variations in modal volume. The final optimized device parameters are:  $S_{1x} = 0.280a$ ,  $S_{2x} = 0.193a$ ,  $S_{3x} = 0.194a$ ,  $S_{4x} = 0.162a$ ,  $S_{5x} = 0.113a$ ,  $S_{1y} = -0.016a$  (i.e. shifted inward), and  $S_{2y} = 0.134a$ , bringing a GME-computed quality factor  $Q_{ideal} = 1.95 \times 10^6$ . Optimization attempts allowing for additional shifts of the off-axis holes and/or variation of the hole-radii did not bring significant improvement. The optimal design is thus mostly determined by variations of positions

of the holes only, which are also the structural features over which the fabrication process ensures the highest precision. The computed mode profile (Fig. 1c) resembles that of the basic  $H0$  design, and most importantly the modal volume remains extremely small:  $V = 0.35 \left( \frac{\lambda}{n} \right)^3$ . We additionally simulated the optimal structure using a finite-element method (COMSOL<sup>TM</sup>), which essentially confirmed the GME-computed values of  $Q$  and  $V$ . The theoretical Q-factor of the present design is nearly one order of magnitude larger than the previously highest reported value<sup>13</sup>, which was obtained through separate optimization of individual hole-positions. This fact highlights the importance of using a global optimization algorithm.

In order to assess the robustness of this design, we modelled random disorder in the form of fluctuations in the hole positions and radii<sup>20,21</sup>, drawn from a Gaussian random distribution with zero mean and standard deviation  $\sigma$ . Fig. 1d and e show histograms – each obtained from the simulation of 1000 disorder realisations – of the probability distribution of Q-values, respectively for two different  $\sigma$  values. Disorder reduces the Q-factor on average, as expected<sup>20,21</sup>. However, very high quality factors for a reasonable fabrication disorder are predicted, proving the robustness of this design in terms of practical applications.

Several nanocavities were fabricated in silicon, following the optimal design, with  $a = 435\text{nm}$  (see methods section). Each nanocavity was located in the proximity of a  $W1$  waveguide, either in a side-coupling (Fig. 1b) or cross-coupling (Fig. 3a) scheme, and was characterized by a different distance to the waveguide

$D = n \frac{\sqrt{3}}{2} a$  ( $n = 5, \dots, 15$ ). When measuring the Q-factors, the input light power was

lowered until optical nonlinearities (see below) vanished and the device operated in a regime of linear response. Cavity emission spectra are shown in Fig 2b and c for  $n = 11$  and  $n = 15$  respectively. Fig. 2a shows the change in measured Q-factor, for the side-coupled cavities, as  $n$  is increased. The variation is due to the coupling waveguide that acts as an additional loss channel for the cavity<sup>12</sup>. A maximum value of  $Q = 418,000$  for a coupling distance  $n = 15$  was measured. The data in Fig. 2a suggest clearly that, at  $n = 15$ , the coupling waveguide still affects the measured Q-factor. A conservative way of extrapolating the “unloaded” Q-factor  $Q_{UL}$  consists in assuming an exponential decay with distance of the cavity-waveguide coupling. More precisely, we assume  $Q^{-1} = Q_{UL}^{-1} + C \exp(-\alpha D)$ . A fit of the measured Q-values (with  $C$ ,  $Q_{UL}$ , and  $\alpha$  as free parameters), as plotted in Fig. 2a, yields  $Q_{UL} = 485000$ , which should be taken as a lower bound to the actual unloaded Q-factor. This value is in very good agreement with the maximum in the histogram of Fig. 1e, computed for a disorder amplitude  $\sigma = 0.003a$ , which is a very reasonable estimate of the largest fluctuations introduced in the fabrication process<sup>25</sup>. Fig. 2a also shows that at short distances, where the Q-factor is still very high ( $\sim 100,000$ ), losses are largely dominated by coupling into the waveguide channel, thus highlighting the potential for photonic applications.

With a measured quality factor  $Q = 418,000$  and a modal volume  $V = 0.35 \left(\frac{\lambda}{n}\right)^3$ , this

$H0$  nanocavity ranks among those with the highest  $\frac{Q}{V}$  ratio ever reported<sup>1,10,11,14,26–29</sup>.

If spatial compactness is taken as an additional requirement, then our measured  $\frac{Q}{V}$ -value exceeds that of existing reports<sup>1,12,14,26</sup> by at least one order of magnitude. The

present  $H0$  design has the advantage of being spatially compact, reproducible and robust to fabrication imperfections.

As a further illustration of the effectiveness of the evolutionary optimization method, we have generated an alternate optimal  $H0$  design with the requirement of a smaller modal volume, imposed by introducing a stricter upper bound  $S_{1x} < 0.25a$ . This results in a design with parameters  $S_{1x} = 0.216a$ ,  $S_{2x} = 0.103a$ ,  $S_{3x} = 0.123a$ ,  $S_{4x} = -0.017a$ ,  $S_{5x} = 0.067a$ ,  $S_{1y} = 0.004a$  and  $S_{2y} = 0.194a$  corresponding to an ideal Q-factor  $Q_{ideal} = 1.05 \times 10^6$  and a smaller modal volume  $V = 0.26 \left( \frac{\lambda}{n} \right)^3$ . This design was also fabricated and experimentally characterized. A maximum Q-factor  $Q = 260,000$  was measured. These two results provide a solid experimental confirmation of the full power of the present optimization technique. Global optimization revolutionises the field of photonic crystal nanocavities by showing that, contrarily to common belief, most cavity designs – and not only few specific structures<sup>8-10</sup> – can be optimized to display ideal quality factors well above one million. We anticipate that, using global optimization we can drastically improve the ideal Q-factor of other simple PhC nanocavity designs. For example, we could improve the Q-factor of a L3 cavity from  $Q_{ideal} = 260'000$ <sup>12</sup> to  $Q_{ideal} = 1.7 \times 10^6$ , and that of a H1 cavity from  $Q_{ideal} = 62'000$ <sup>14</sup> to  $Q_{ideal} = 1.1 \times 10^6$ , just by varying the same free parameters as in those previous studies.

The  $\frac{Q}{V}$  ratio is a measure of the enhancement of optical nonlinearities produced by the cavity<sup>22,26,30</sup>. Fig. 3a shows the nonlinear behaviour, as a function of input power,

of the emission spectrum of a cavity with measured Q-factor  $Q = 150,000$  and cross-coupling configuration (which simplifies the estimation of the intracavity power, see supplementary information). At low power, a slight blue shift of the cavity mode is observed and attributed to free carrier dispersion<sup>26</sup>. Starting at  $0.6\mu W$ , heating due to nonlinear absorption, and optical-Kerr nonlinearity result in a redshift. At higher input powers, a drop in the spectral response on the red side of the resonance indicates the onset of optical bistability. To characterize this bistable behaviour, we sweep the input power and record the steady-state emission intensity. Figs. 3b and c show hysteresis plots, respectively for an excitation wavelength red-shifted by 20 pm and 40 pm from the cavity resonance. Switching power ratios  $\left(\frac{P_{up}}{P_{down}}\right)$  of respectively 2.0 ( $P_{up} = 26\mu W$  and  $P_{down} = 13\mu W$ ) and 4.5 ( $P_{up} = 90\mu W$  and  $P_{down} = 20\mu W$ ), and a contrast above 70% are obtained, demonstrating robust and controllable bistable behaviour. The present cavity displays the lowest power threshold for optical bistability ever measured in 2D PhC silicon devices<sup>4,31</sup>.

A high  $Q$ -factor and a small modal volume are not the only important requirements in view of applications. Many photonic structures of current interest, such as e.g. coupled cavities or coupled-resonator waveguides<sup>4</sup>, rely on spatial proximity between two cavities or one cavity and one waveguide, while in a longer-term perspective the density of optical elements will represent a key figure of merit of photonic circuits. The ability to produce small compact cavities like e.g.  $Hn$  or  $Ln$  structures with record-high  $Q$ -factors – as made possible by our optimization procedure – thus constitutes a major advance in view of an integrated photonic technology.

In summary, we have developed a global optimization procedure for PhC nanocavities, that can drastically improve the  $Q$ -factor of common moderate- $Q$  designs by just varying a few structural parameters. Thanks to this procedure, we have demonstrated a novel ultrasmall PhC nanocavity with a measured  $Q$ -factor of 418,000 and a  $\frac{Q}{V}$ -ratio exceeding  $10^6 \left(\frac{\lambda}{n}\right)^{-3}$ , ranking among the topmost values ever demonstrated in 2D PhC structures. The cavity displays optical bistability at a threshold power of  $13\mu W$ , the lowest ever reported for a silicon device. These features, combined with the compact design, make this cavity an ideal candidate element for silicon photonic integrated circuits. It also holds great promise as a platform for solid-state cavity quantum electrodynamics, where a high  $\frac{Q}{V}$  ratio is the main requirement to achieve single-photon nonlinearities for quantum information applications<sup>7</sup>. The evolutionary optimization that brought to this design promises to play a major role in the future development of customizable PhC cavity devices for specific application requirements.

**Methods summary:**

2D Photonic crystal devices are fabricated on a SOITEC Silicon-On-Insulator wafer, which consists of a 220 nm thick silicon layer and a 2- $\mu\text{m}$  thick silica ( $\text{SiO}_2$ ) layer on a silicon substrate. The photonic crystal pattern is defined with electron beam lithography (VISTEC EBPG5000) on an electro-sensitive resist (ZEP520) and the developed pattern is further transferred into the silicon layer with an inductively coupled plasma (ICP) AMS200 dry etcher with a  $\text{SF}_6$  and  $\text{C}_4\text{F}_8$  gas mixture. The last step is the removal of the sacrificial  $\text{SiO}_2$  layer with buffered HF (BHF) wet etching.

**Acknowledgements**

The authors acknowledge the financial support from the Swiss National Centre of Competence in Research Quantum Photonics and the Swiss National Science Foundation projects n° 200021\_134541 and 200020\_132407. We also acknowledge Dario Gerace for fruitful discussions during the progress of the work.

**Author Contributions**

MM and VS carried out the theoretical part of this work, developed and implemented the simulation tool, and carried out the optimization procedure leading to the basic cavity designs. UD, MT, and RH carried out the fabrication and experimental part of the work, UD carried out the additional finite-element simulations. All authors equally contributed to the preparation of the manuscript.

## References

1. Nozaki, K. *et al.* Sub-femtojoule all-optical switching using a photonic-crystal nanocavity. *Nat. Photonics* **4**, 477–483 (2010).
2. Nozaki, K. *et al.* Ultralow-power all-optical RAM based on nanocavities. *Nat. Photonics* **6**, 248–252 (2012).
3. Takahashi, Y. *et al.* A micrometre-scale Raman silicon laser with a microwatt threshold. *Nature* **498**, 470–474 (2013).
4. Notomi, M. Manipulating light with strongly modulated photonic crystals. *Reports Prog. Phys.* **73**, 096501 (2010).
5. Vučković, J., Lončar, M., Mabuchi, H. & Scherer, A. Design of photonic crystal microcavities for cavity QED. *Phys. Rev. E* **65**, 016608 (2001).
6. Yoshie, T. *et al.* Vacuum Rabi splitting with a single quantum dot in a photonic crystal nanocavity. *Nature* **432**, 200–203 (2004).
7. Reinhard, A. *et al.* Strongly correlated photons on a chip. *arXiv:1108.3053* (2011). doi:10.1038/nphoton.2011.321
8. Song, B.-S., Noda, S., Asano, T. & Akahane, Y. Ultra-high-Q photonic double-heterostructure nanocavity. *Nat. Mater.* **4**, 207–210 (2005).
9. Tanabe, T., Notomi, M., Kuramochi, E., Shinya, A. & Taniyama, H. Trapping and delaying photons for one nanosecond in an ultrasmall high-Q photonic-crystal nanocavity. *Nat. Photonics* **1**, 49–52 (2007).
10. Taguchi, Y., Takahashi, Y., Sato, Y., Asano, T. & Noda, S. Statistical studies of photonic heterostructure nanocavities with an average Q factor of three million. *Opt. Express* **19**, 11916–11921 (2011).
11. Akahane, Y., Asano, T., Song, B.-S. & Noda, S. High-Q photonic nanocavity in a two-dimensional photonic crystal. *Nature* **425**, 944–947 (2003).
12. Akahane, Y., Asano, T., Song, B.-S. & Noda, S. Fine-tuned high-Q photonic-crystal nanocavity. *Opt. Express* **13**, 1202–1214 (2005).
13. Nomura, M., Tanabe, K., Iwamoto, S. & Arakawa, Y. High-Q design of semiconductor-based ultrasmall photonic crystal nanocavity. *Opt. Express* **18**, 8144–8150 (2010).
14. Takagi, H. *et al.* High Q H1 photonic crystal nanocavities with efficient vertical emission. *Opt. Express* **20**, 28292–28300 (2012).
15. Zhang, Z. & Qiu, M. Small-volume waveguide-section high Q microcavities in 2D photonic crystal slabs. *Opt. Express* **12**, 3988–3995 (2004).
16. Husko, C. *et al.* Ultrafast all-optical modulation in GaAs photonic crystal cavities. *Appl. Phys. Lett.* **94**, 021111–021111–3 (2009).
17. Englund, D., Fushman, I. & Vučković, J. General recipe for designing photonic crystal cavities. *Opt. Express* **13**, 5961–5975 (2005).
18. Kuramochi, E. *et al.* Ultrahigh-Q photonic crystal nanocavities realized by the local width modulation of a line defect. *Appl. Phys. Lett.* **88**, 041112 (2006).
19. Felici, M., Atlasov, K. A., Surrente, A. & Kapon, E. Semianalytical approach to the design of photonic crystal cavities. *Phys. Rev. B* **82**, 115118 (2010).
20. Portalupi, S. L. *et al.* Deliberate versus intrinsic disorder in photonic crystal nanocavities investigated by resonant light scattering. *Phys. Rev. B* **84**, (2011).
21. Hagino, H., Takahashi, Y., Tanaka, Y., Asano, T. & Noda, S. Effects of fluctuation in air hole radii and positions on optical characteristics in photonic crystal heterostructure nanocavities. *Phys. Rev. B* **79**, 085112 (2009).

22. Uesugi, T., Song, B.-S., Asano, T. & Noda, S. Investigation of optical nonlinearities in an ultra-high-Q Si nanocavity in a two-dimensional photonic crystal slab. *Opt. Express* **14**, 377–386 (2006).
23. Descharmes, N., Dharanipathy, U. P., Diao, Z., Tonin, M. & Houdré, R. Observation of Backaction and Self-Induced Trapping in a Planar Hollow Photonic Crystal Cavity. *Phys. Rev. Lett.* **110**, 123601 (2013).
24. Andreani, L. C. & Gerace, D. Photonic-crystal slabs with a triangular lattice of triangular holes investigated using a guided-mode expansion method. *Phys. Rev. B* **73**, 235114 (2006).
25. Le Thomas, N., Diao, Z., Zhang, H. & Houdré, R. Statistical analysis of subnanometer residual disorder in photonic crystal waveguides: Correlation between slow light properties and structural properties. *J. Vac. Sci. Technol. B Microelectron. Nanometer Struct.* **29**, 051601 (2011).
26. Barclay, P., Srinivasan, K. & Painter, O. Nonlinear response of silicon photonic crystal microresonators excited via an integrated waveguide and fiber taper. *Opt. Express* **13**, 801–820 (2005).
27. Deotare, P. B., McCutcheon, M. W., Frank, I. W., Khan, M. & Lončar, M. High quality factor photonic crystal nanobeam cavities. *Appl. Phys. Lett.* **94**, 121106–121106–3 (2009).
28. Takahashi, Y., Tanaka, Y., Hagino, H., Asano, T. & Noda, S. Higher-order resonant modes in a photonic heterostructure nanocavity. *Appl. Phys. Lett.* **92**, 241910–241910–3 (2008).
29. Asano, T., Song, B.-S. & Noda, S. Analysis of the experimental Q factors ( $\sim 1$  million) of photonic crystal nanocavities. *Opt. Express* **14**, 1996–2002 (2006).
30. Notomi, M. *et al.* Optical bistable switching action of Si high-Q photonic-crystal nanocavities. *Opt. Express* **13**, 2678–2687 (2005).
31. Zhang, Y. *et al.* Ultralow Power Nonlinear Response in an Si Photonic Crystal Nanocavity. *IEEE Photonics J.* **5**, 6601409–6601409 (2013).

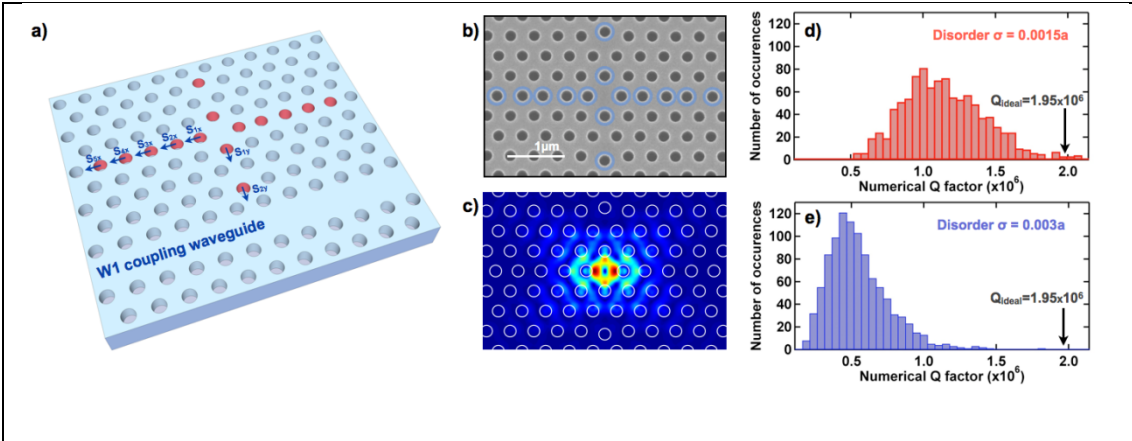


**Figure 1| The optimized ultra-high Q H0 nanocavity**

**a**, The schematic of the proposed design, highlighting (in red) the holes whose positions have been optimized. The coupling W1 waveguide, at a distance  $D = 5a\sqrt{3}/2$  from the cavity, is shown. The displacement parameters are labelled and indicated by arrows. **b**, Scanning electron micrograph of one of the fabricated cavities, with the displaced holes encircled in blue for clarity. **c**, Electric field distribution in the cavity as computed with the guided mode expansion method. **d and e**, Histograms of the computed quality factor in the presence of random structural disorder, respectively for disorder parameters  $\sigma = 0.0015a$  and  $\sigma = 0.003a$ . The ideal Q-factor without disorder for this cavity is computed to be  $Q_{ideal} = 1.95 \times 10^6$  and is indicated in both plots.

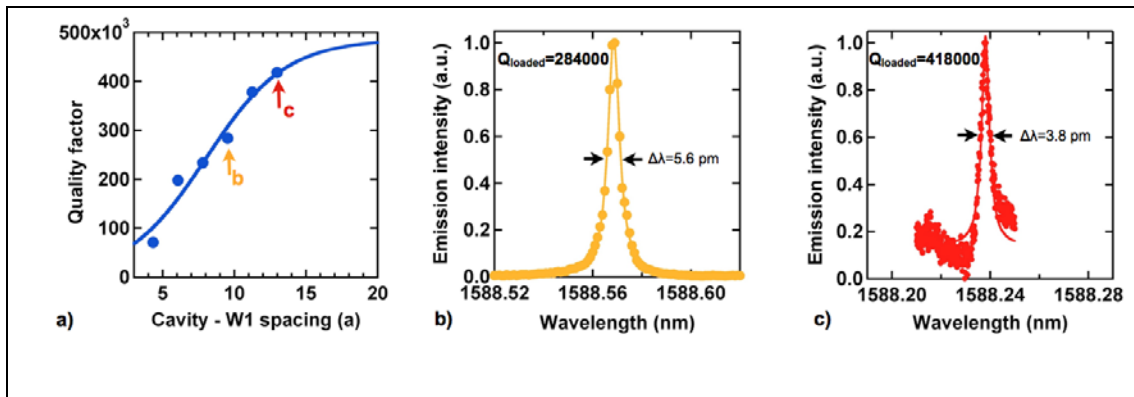


**Figure 2| Experimental measurement of the quality factors in the linear regime**

**a**, The change in the measured Q-factor as the distance from the side coupling W1 waveguide is increased. The blue line shows the best fit of the experimental data to the model discussed in the text, indicating an unloaded Q-factor  $Q = 485,000$ . **b and c**, Cavity emission spectra measured for two values of the cavity-waveguide distance, indicated by arrows in panel **a**. The experimental data are fitted with a Lorentzian curve (also shown) and the extracted full width at half maximum results respectively in quality factors  $Q = 284,000$  and  $Q = 418,000$ .

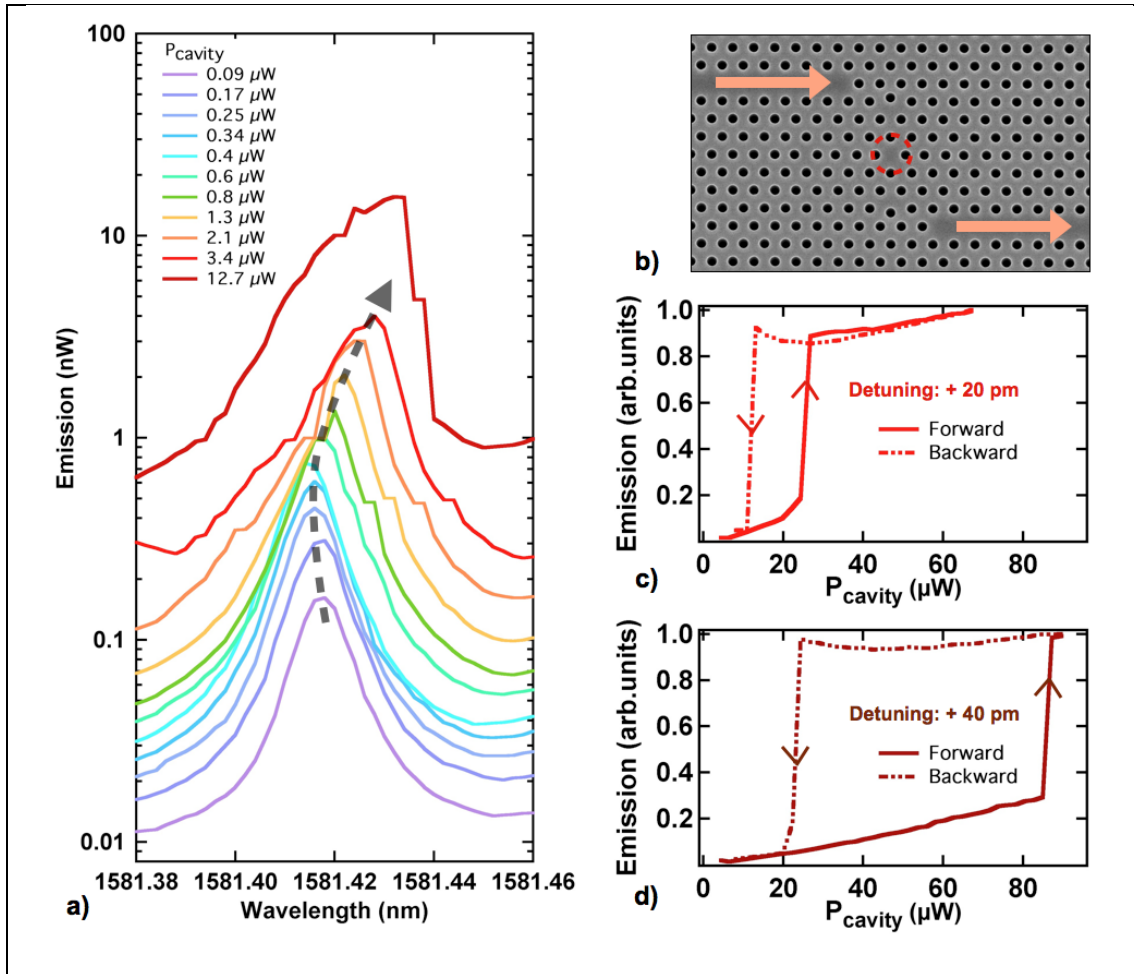


**Figure 3| Demonstration of low-power nonlinear response and optical bistability**

**a**, Measured emission spectrum from the cavity, as the input power is increased. The dashed line is a guide to the eye to indicate the change in the resonance wavelength. At low input power, there is a blue shift of the resonance as the input power is increased, which at higher input power gradually turns into a strong red shift, which is attributed to thermal nonlinearities implied by two-photon absorption. A marked asymmetry in the cavity spectral signature for the largest values of the input power indicates the onset of bistable behaviour. **b**, Scanning electron micrograph of the cross-coupled cavity structure used to measure optical nonlinearities. **c** and **d**, The bistability is probed by sweeping the input power and recording the steady state emission from the cavity. A clear hysteresis is observed with a large contrast and very low power threshold. Panels **b** and **c** show data measured respectively with the input laser detuned by 20pm and 40pm above the cavity resonant wavelength.

# **Evolutionarily optimized ultrahigh-Q photonic crystal nanocavity**

**(Supplementary Information)**

## **The Genetic-Optimization method**

The objective function that has been optimized with the stochastic evolutionary algorithm is the Q-factor – computed with the guided-mode expansion method [1] – for a single realization of hole positions. It should be noted that this choice is not unique but rather highly customizable. Since a single computation yields both Q and the electromagnetic mode profile, it would be equally straightforward to optimize Q/V for example, or even more specific quantities like the amount of electric field penetrating into air. The stochastic evolutionary algorithm used here is the one included in the MATLAB<sup>®</sup> Global Optimization Toolbox [2], which starts from a random initial population and goes on to create a sequence of generations where the fittest (highest-Q) individuals are kept, while mutation, crossover and migration among separate populations are used to create the offspring forming the next generation. Reasonable constraints on the shifts are imposed: for the initial H0 optimization, the absolute value of the shift was set to be smaller than  $0.3a$ . For the design with a smaller mode volume, this boundary was decreased to  $0.25a$ . For both designs, a rough optimization was first performed with large allowed range of variation of all parameters, which was then followed by a fine-tuning optimization in which smaller variations around the rough optimal values were allowed. This ensures convergence within approximately 200 generations in total, with 120 individuals in each generation.

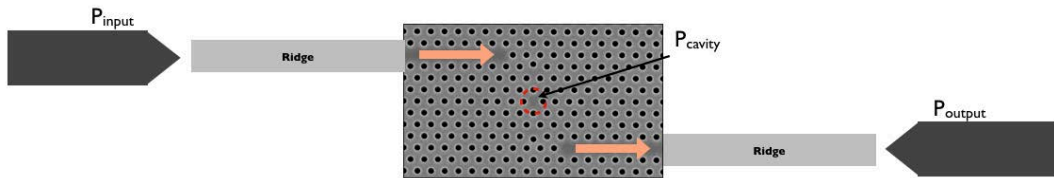
### **Computation of modal volumes**

The modal volumes  $V$ , for all the cavity designs investigated in this work, were calculated both using guided-mode expansion and with the help of a 3D Finite element solver. The following definition of the modal volume – coinciding with that used in the works quoted in Table 1 – was used

$$V = \frac{\int \varepsilon(\vec{r}) |\vec{E}(\vec{r})|^2 d^3r}{\max[\varepsilon(\vec{r}) |\vec{E}(\vec{r})|^2]} \quad (1)$$

where  $\varepsilon(\vec{r})$  is the spatial profile of the dielectric permittivity and  $\vec{E}(\vec{r})$  is the electric field associated to the cavity mode.

### **Estimation of power in the cavity for measurements of nonlinear effects**



**Supplementary Figure 1** | Sketch of the coupling scheme implemented for the measurements of nonlinear effects.

The devices are coupled to an input laser and a detector on the output side in a typical endfire configuration. The cavities are coupled with a cross-coupling configuration as shown in Supplementary Fig. 1., which creates a symmetric system with the cavity in the centre. This facilitates the use of the following method to estimate the power in

the cavity. For a known input power, the power in the centre of such a system is given by

$$P_{cavity} = \sqrt{T}P_{input} = \sqrt{\frac{P_{output}}{P_{input}}}P_{input} = \sqrt{P_{input}P_{output}} \quad (2)$$

For the cavity used for the characterization of nonlinear effects we measure a transmission power  $P_{output} \sim 2nW$  in the detector, at the resonance wavelength, for an input power  $P_{input} = 4\mu W$ , corresponding to  $P_{cavity} = 0.09\mu W$ , for which the system response is still in the linear regime. The values of  $P_{cavity}$  for increasing input powers were linearly extrapolated from this value.

## References

- [1] L. C. Andreani and D. Gerace, Physical Review B **73** (2006).
- [2] MATLAB and Global Optimization Toolbox Release 2012b, The MathWorks, Inc., Natick, Massachusetts, United States.